2012 ASME International Manufacturing Science and Engineering Conference
MSEC2012
June 4-8, 2012, Notre Dame, Indiana, USA

MSEC2012-7276

CHARACTERIZATION OF CUTTING FORCE INDUCED SURFACE SHAPE VARIATION USING HIGH-DEFINITION METROLOGY

Hai Trong Nguyen, Hui Wang, S. Jack Hu
Department of Mechanical Engineering, University of Michigan
Ann Arbor, Michigan, USA

ABSTRACT

High-definition metrology (HDM) systems with fine lateral resolution are capable of capturing the surface shape on a machined part that is beyond the scope of measurement systems employed in manufacturing plants today. Such surface shapes can precisely reflect the impact of cutting processes on surface quality. Understanding the cutting processes and the resultant surface shape is vital to identifying opportunities for high-precision machining process monitoring and control. This paper presents modeling and experiments of a face milling process to extract surface patterns from measured HDM data and correlate these patterns with cutting force variation. A relation is established between instantaneous cutting forces and the observed dominant patterns along the feed and circumferential directions. Potential applications of such relationship in process monitoring, diagnosis, and control are also discussed.

Keywords: machined surface, cutting force, surface characterization

INTRODUCTION

Surface shapes have a crucial impact on product functions and it has been difficult to precisely characterize the detailed surface shape using measurement devices employed in manufacturing plants today. For example, in the automotive industry, surface shape variation surrounding the bores on a deck face of an engine head may affect the sealing between the deck face and head gasket during the subsequent assembly. To capture these variation efficiently, metrology techniques that can scan large surfaces with micron-level resolution are needed.

Various surface metrology techniques have been developed over the past several decades, including contact and noncontact techniques. The contact surface metrology uses a stylus, probe, or retroreflector to scan a surface and the non-contact metrology systems employ optical methods. Extensive reviews on these techniques are given by Huynh et al. [1] and Whitehouse [2].

The disadvantage of these techniques is a lack of efficiency in measuring large surfaces with high resolution. The conventional high resolution metrology systems have very limited scanning range and required long measurement time. For the contact metrology system, though the scanning range can be up to hundreds or thousands of millimeters, the contact mechanism usually requires significant amount of time in scanning large complex surfaces. Furthermore, the tip size associates with certain contact scanning systems can lead to reduced lateral resolution, rendering it difficult to precisely obtain fine-scale surface information. The noncontact metrology system that can characterize a large area usually has a poor vertical resolution such as an optical CMM.

Recently, a new type of high-definition metrology (HDM) system has been developed to inspect surfaces with high resolution along the vertical and lateral directions. Such a system is capable of measuring large 3D surfaces using laser holographic interferometry (LHI) [3-4]. For example, within 1-2 minutes, it can collect 4-million data points from an area of up to $300\times300mm^2$. Figure 1 qualitatively compares the inspection range, and lateral resolutions between LHI based HDM and common in-plant surface gages such as CMM and conventional HDM such as 3D stylus-based profilometer, optical profilometer, 3D-microscope [5]. It can be seen that the LHI system achieves a 150 μm lateral resolution at a relatively high scanning speed. As such, it offers measurement capability that fills the gap between profilometer and CMM.

Figure 2 shows the HDM image of a deck face on an engine head. The aforementioned surface height variation surrounding the cylinder bores can be clearly observed. These surface distortions can be captured at multiple length scales, from millimeters to decimeters, depending on the workpiece size as well as the cutter geometry. Such patterns impact the functional performances and the HDM represents new opportunities for the understanding the cutting process and improving quality in high-precision machining.

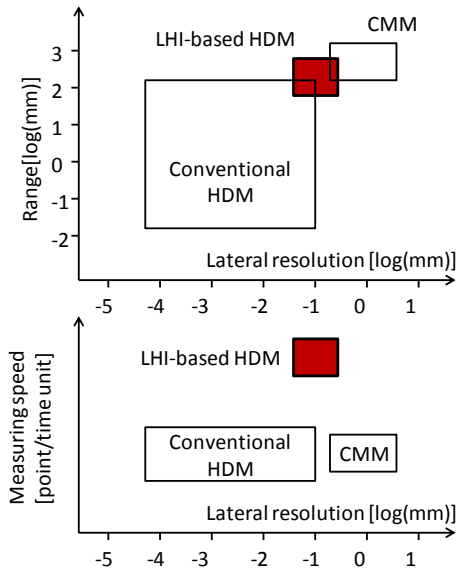

FIG. 1 COMPARISON AMONG LHI BASED HDM, CONVENTIONAL HDM, AND CMM IN PLANTS

FIG. 2 A FACE MILLED SURFACE MEASURED BY THE LHI

Machined surface patterns have been extensively studied in multiple scales. At fine scales (micron level), surface textures were correlated to a number of process conditions. Tool conditions were found to have a significant impact on surface texture, (Wilkison et al. [6] and Yi et al. [7]). Schmitz et al. [8] correlated tool runout, stability, and surface location errors to surface finish. Baek at al. [9] introduced a model to predict surface roughness that includes cutting conditions, edge profile, insert runout, and dynamic characteristics. Kline et al. [10] showed the effects of radial runout and chipload on surface finish. Surface errors were also predicted along with cutting force considering system deflections (Sutherland et al. [11]). At coarse scales (from several millimeters to the form), Takeuchi et al. [12] studied the effects of spindle tilt and thermal expansion on the surface form error. Camelio et al. [13] investigated the effect of fixturing and clamping on surface form error. Liao at al. [14] used FEM to model fixture-workpiece to study the influence of clamping preload and machining force on the machined surface quality. Gu et al. [15] used a finite element method called equivalent flexibility influence coefficient to predict the deformation of cutter-spindle and workpiece-fixture assembly. The relative position between cutter and workpiece can be predicted to estimate surface errors.

A number of models have been developed to estimate cutting forces in machining. Ruzhong et al. [16] characterized cutting force profile in face milling based on single tooth cutting. Wang et al. [17] developed a convolution modeling method to predict the total cutting force in milling. Anderson et al. [18] studied how the cutting action of an insert is affected by neighboring inserts. Li et al. [19] predicted cutting forces of dynamic milling processes considering thermal effect. Wu [20] studied the dynamic cutting process by developing the transfer function between the vibration variables and the dynamic force components for a single degree-of-freedom machining system. Montgomery et al. [21] studied the effect of cutting dynamics on surface finish and established a relation between tooth passing frequency and a dominant frequency of tool-workpiece structure.

Due to a lack of metrology that is capable of measuring large surfaces with high resolution, the surface patterns such as those reflected by the HDM data in Fig. 2 have not been studied in the previous research. Based on the LHI technology, this paper identifies surface distortion patterns and establishes the correlation with material removal rate. The shape patterns are extracted along the feed and circumferential directions of cutter movement. Along the circumferential direction, the cutting force variation due to different engagement of inserts with cutting is analyzed and correlated to surface patterns. Along the feed direction, the surface variation is compared with the cutting force changes due to the variations in material removal rate (MRR). The relationship between the MRR and surface height is quantified to characterize the shape patterns in this direction. Finally, we discuss the potential applications of the extracted surface patterns as well as new parameters/metrics that can be derived for process monitoring and product/process improvement.

The remainder of the paper is organized as follows. We first describe the experiments and surface shape pattern extraction along the feed and circumferential directions, then conduct cutting force modeling along the two directions to interpret the shape patterns and discuss applications of the extracted surface characteristics in process monitoring and improvement. Conclusions are given in the last section.

EXPERIMENTS AND EXTRACTION OF SHAPE PATTERNS

Experiments are conducted to analyze the surface patterns along the feed and circumferential directions based on the HDM data, respectively. Spline filtering method is selected to extract the patterns.

Experiment setup

Face milling is used to cut the three solid blocks of Aluminum 2024-T351 with dimensions of 75x270x75 mm^3 (Fig. 3). The large thickness value (75mm) is chosen to reduce the structural deformation. The depth of cut is 0.5mm; the feed rate is 0.5 mm/tooth; and the spindle speed is 1000 rev/min. The cutter has an effective diameter of 101.6 mm with five inserts. The face milling operation was implemented on a Cincinnati CNC machine (model HMC-400EP) and the machined surfaces were measured by a ShaPix^{TM} laser holographic interferometer.

In this experiment, three blocks with different surface designs were prepared to investigate the impact of the MRR on surface profiles. The MRR determines the axial cutting force and is directly influenced by the surface design such as size, shape, and spatial distribution of holes. Block 1 is solid (Fig. 4.a) which is used to study the variation of surface height along the circumferential direction. Block 2 (Fig. 4.b) has pockets whose curved edge has the same radius as that of the cutter. This surface design will cause drastic change of the MRR (volume of materials removed per revolution of the cutter) as the cutter moves along the feed direction. The Block 3 (Fig. 4.c) has holes with different diameters. This design can lead to a smoother change of MRR along the feed direction.

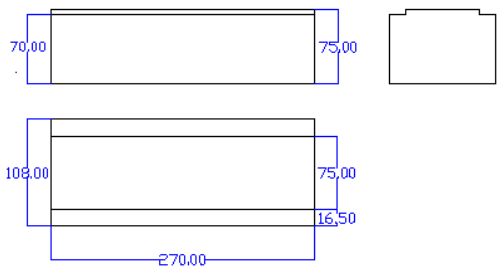

FIG. 3 DIMENSIONS OF THE ALUMINUM BLOCKS (MM)

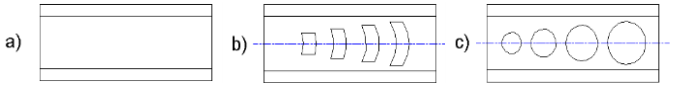

FIG. 4 GEOMETRIES OF THE WORKPIECE (a – BLOCK 1, b – BLOCK 2, c – BLOCK 3)

Selection of filtering algorithm and image preprocessing

A machined surface has patterns with a wide range of spatial frequencies including roughness/ waviness (short wavelength) and form (large wavelength) [22]. Patterns at different frequencies are mainly extracted by using filtering methods [23] such as 2RC filter, Gaussian filter, Rk filter, spline filter, robust spline filter, Gaussian regression and robust Gaussian regression filters, and morphological filter. Spline filtering method is chosen for surface pattern extraction due to its efficiency in image processing with less boundary distortion and its robustness against outlier compared with other filtering methods.

To facilitate the filtering along the circumferential direction, the toolmark is first straightened by using a mapping function that maps points on insert trajectory curve to corresponding points on a straight line. Then the filtering is applied to the straightened profile. Fig. 5.a shows the toolmark produced by one insert on one revolution. The cutter path is along the horizontal axis (X direction). The cutting point A rotates about the cutter center O_c which is moving along the cutter path. The front of the leading edge of the cutter is at D. Assume that the cutter moves along the X axis at the feed rate f (mm/s) and rotates at the speed of ω (ω = πS/30 (rad/s)), where S is the spindle speed (rev/min)). Assume that the cutting point start at a point A (t=0). At a given time *t*, the coordinates of the cutting point B are

$$\begin{aligned} X_B &= X_{Oc} + ft + R\sin\omega t \\ Y_B &= R\cos\omega t \end{aligned} \quad (1)$$

The time elapsed when the cutting point reaches the point B is $t_B = (\pi/\omega)\cos(Y_B/R)$. So, $XO_c = X_B - ft_B - R\sin\omega t_B$. When $\omega t = \pi/2$ (point D), one can have $t_D = \pi/(2\omega)$ and $OC_D = ft_D + R$. The projection plane can be any plane that perpendicular to the feed direction. It can be chosen to pass through point D for simplifying the calculation. The coordinates of the point (C) on the straightened path corresponding to the point B can be calculated by

$$X_C = X_{Oc} + O_C D = X_B + f\left(\frac{\pi}{2\omega} - t_B\right) + R(1 - \sin\omega t_B) \quad (2)$$

$$Y_C = \begin{cases} \int_{t_P}^{t_D} \sqrt{\left(\frac{dx}{dt}\right)^2 + \left(\frac{dy}{dt}\right)^2}\,dt = \int_{t_P}^{t_D} \sqrt{\left(f + \omega R\cos\omega t\right)^2 + \left(R\sin\omega t\right)^2}\,dt, & 0 < \theta < \pi/2 \\ -\int_{t_D}^{t_P} \sqrt{\left(f + \omega R\cos\omega t\right)^2 + \left(R\sin\omega t\right)^2}\,dt, & \pi/2 < \theta < \pi \end{cases} \quad (3)$$

where θ is defined in Fig. 5. Using equations (2) and (3), the toolmark can be straightened by mapping all points along the toolmark onto a straight path as shown in Fig. 5.b-c.

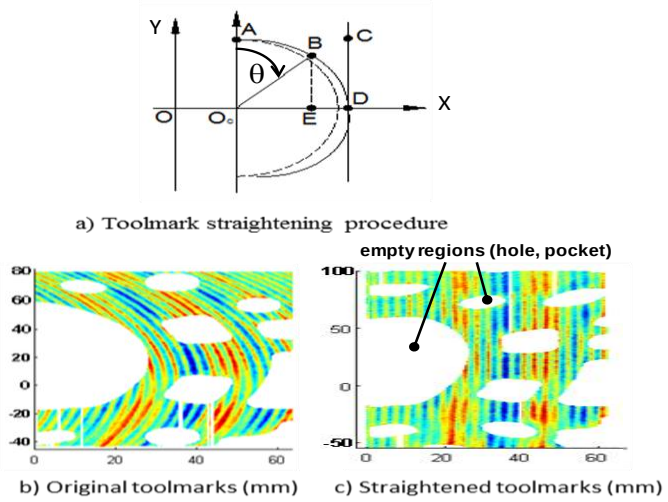

FIG. 5 TOOLMARK STRAIGHTENING

Results

The measured surfaces of blocks 1, 2, and 3 are shown in Fig. 6. The surface of Block 1 (Fig. 6.a-b) exhibits a high-low-high pattern in the circumferential direction whereas there is a lack of obvious pattern along the feed direction. The surface of Block 2 (Fig. 6.b) shows a pattern varying with the surface geometry design, i.e., the surface profile tends to be high where there more materials present without holes (higher MRR) and becomes low where the holes present (low MRR). The measured surface of Block 3 (Fig. 6.c) shares the similar pattern with Block 2. The only difference is that Block 2 shows a sharp profile jump near the edge of holes while the jump in Block 3 is smaller.

Surface patterns along the circumferential direction

The surface pattern along the circumferential direction is shown in Fig. 7. Figures 7.a-e display the insert engagement at different rotational angles of the cutter. Figure 7.a shows the state when only insert 1 is engaged with the cutting. Then insert 5 begins to cut the part while insert 1 is still in cutting (Fig. 7.b). As the cutter rotates, both insert 5 and insert 1 are in cutting (Fig. 7.c). Figure 7.d shows the state when insert 1 exits the part while insert 5 is engaged in cutting. The boundary between the zones with different grey scales in Fig. 7.f outlines the locations where the number of insert engaged in the cutting switches from one to two or from two to one.

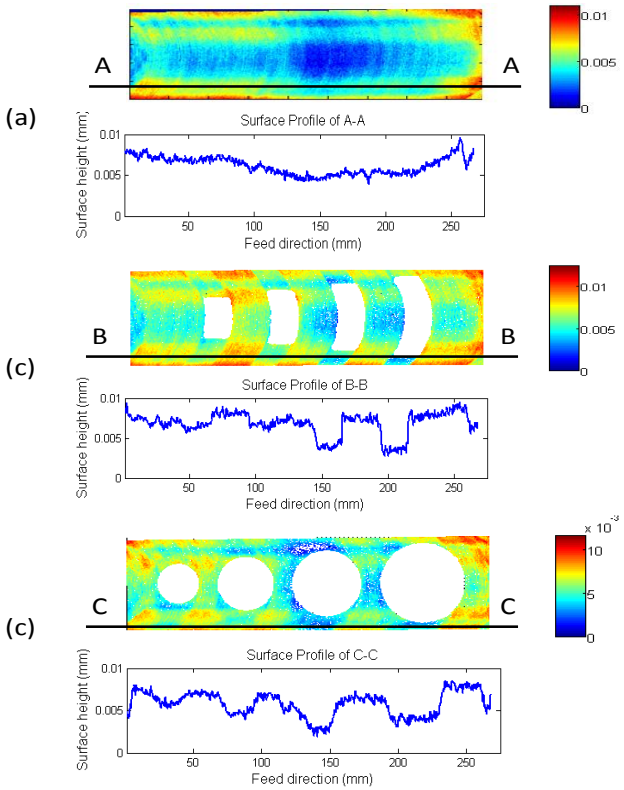

FIG. 6 THE MEASURED SURFACE AND SURFACE PROFLIE OF BLOCK 1, 2, AND 3 (a– BLOCK 1, b– BLOCK 2, c– BLOCK 3)

The surface patterns in the circumferential direction can be extracted by suppressing the surface height variation in the feed direction caused by geometry complexity. A high-pass filter is applied to the surface data along the circumferential direction to extract patterns at the wavelength less than the distance between inserts. The distance between inserts in the circumferential direction equals $2\pi R/N$ = 63.4 mm, where R is the radius of cutter and N is number of inserts. Thus, the cut-off wavelength of the high-pass filter is chosen to be 70 mm. In addition, a low-pass filter with a cut-off wavelength of 7 mm is used to remove fine-scale waviness pattern that is not the focus of this study. The result is shown in Fig. 8.

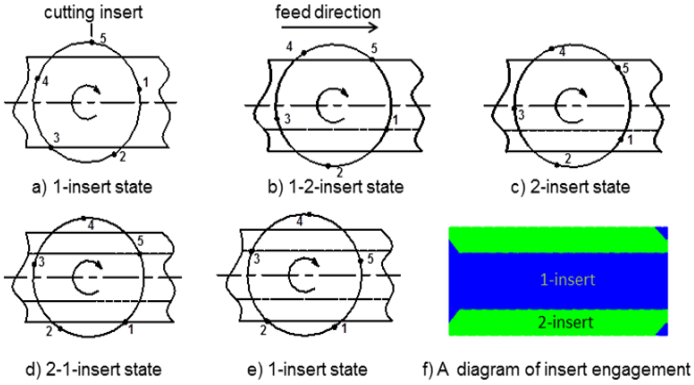

FIG. 7 A DESCRIPTION OF CUTTING INSERT ENGAGEMENT

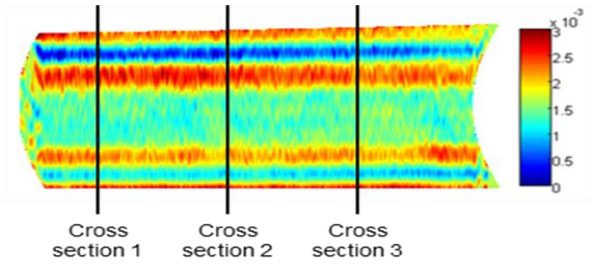

FIG. 8 THE EXTRACTED SHORT WAVELENGTH PATTERNS WITH TOOLMARKS STRAIGHTENED

The extracted pattern as shown in Fig. 8 shows strong similarity with the insert-engagement diagram (Fig. 7) which describes areas of different cutting insert engagement on the surface. Three cross sections from Fig. 8 are plotted in Fig. 9 which shows that the area where the number of inserts engaged in the cutting switches between 1 to 2 has a jump in the profile. In addition, the distance between the peaks is close to that between the boundaries where the number of engaged inserts switches (approximately 42 mm). This phenomenon is caused by the cutting force variation along the circumferential direction and will be modeled in the next section. The same data processing procedure is applied into the surfaces of block 2 and 3 (Fig. 10). The similar high-low patterns are observed.

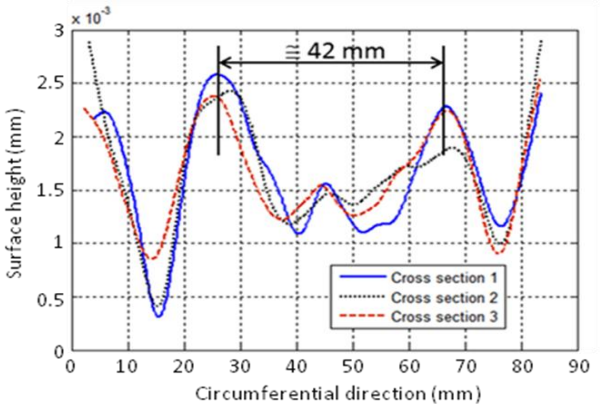

FIG. 9 PROFILES OF THE SHORT WAVELENGTH PATTERN ON BLOCK 1

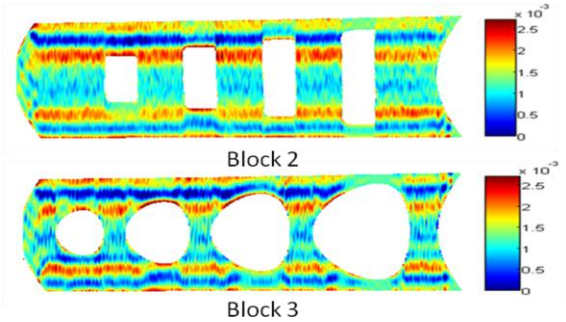

FIG. 10 THE SHORT WAVELENGTH PATTERN ON BLOCK 2 AND 3

Patterns along the feed direction

To extract the surface pattern along the feed direction, the surface height variation in the circumferential direction needs to be suppressed. A low-pass filter is applied at the cutoff wavelength of 75 mm and the surface profile along the circumferential direction is averaged. The resultant pattern after the filtering is shown in Fig. 11. Figure 12 and 13 are the scatter plots for the average height in the circumferential direction and normalized MRR. A positive correlation between the two variables is clearly presented.

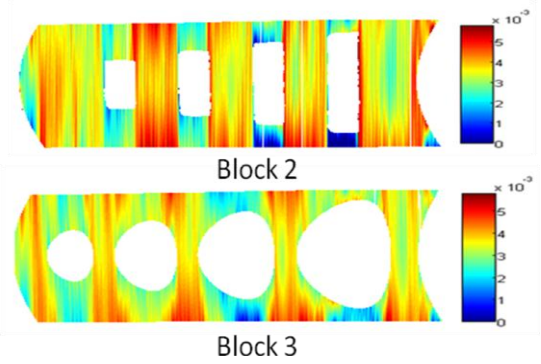

FIG. 11 THE EXTRACTED PATTERN ALONG THE FEED DIRECTION (TOOLMARKS STRAIGHTENED)

In summary, there exist relations between insert engagement, material removal rate (or surface geometry design) and surface profile. The next section will conduct cutting force modeling to explain the mechanism that generates these patterns.

CUTTING FORCE MODELING AND ITS CORRELATION WITH SHAPE VARIATION

In this section, the axial cutting force is modeled and correlated to surface profile along the feed and circumferential directions, respectively. The modeling result is then validated based on the experimental data.

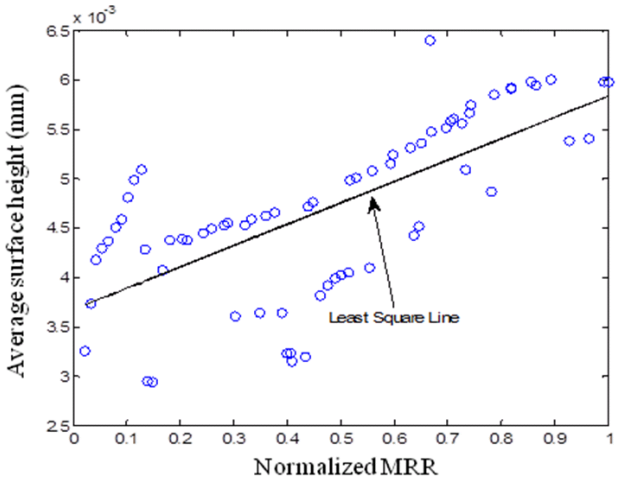

Block 2

FIG. 12 SURFACE HEIGHT VS. MRR ON BLOCK 2

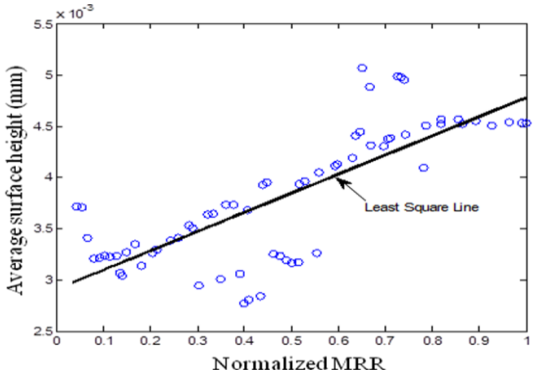

Block 3

FIG. 13 SURFACE HEIGHT VS. MRR ON BLOCK 3

Model Development

Cutting force is one of the main factors that contribute to surface variations. As such, axial cutting force modeling is conducted to estimate the cutter-workpiece relative displacement.

Assume that the machine tool has a very small spindle tilt (less than 0.001 radian) and the depth of cut is considered a constant. It is also assumed that there is no relative displacement between inserts on the cutter.

Figure 14 shows the motion of the cutter relative to the workpiece as well as directions of the cutting forces exerted on each insert. The axial cutting force is the product of cross section area on the chip and the specific cutting pressure K_a which includes all the factors related to cutter geometry, cutter material, and workpiece material [11, 24]. Thus, the axial cutting force acting on insert i can be estimated by

$$F_{ai} = K_a f_t \sin(\theta_i(\phi)) d \tag{4}$$

where $\theta_i(\phi)$ is the rotation angle of insert i when the cutter rotates at an angle ϕ; f_t is the feed rate per tooth; and d is the depth of cut.

With N cutting inserts, the total amount of axial cutting force applied on the cutter at certain insert angle θ is

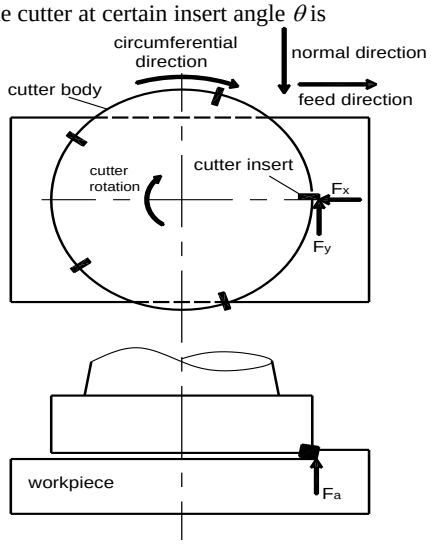

FIG. 14 THE CUTTING FORCE DIAGRAM FOR THE CUTTER-WORKPIECE SYSTEM

$$F_a = \sum_{i=1}^{N} \delta(\theta_i(\phi)) F_a(i,\phi) = K_a d \sum_{i=1}^{N} \delta(\theta_i(\phi)) C_i(\theta_i(\phi)) = K_a d f_t \sum_{i=1}^{N} \delta(\theta_i(\phi)) \sin\theta_i(\phi) \quad (5)$$

where $\delta(\theta_i)$ is an indicator function that implies whether or not the insert i is engaged in a cutting process, i.e. [11],

$$\delta(\theta_i(\phi)) = \begin{cases} 1 & if \quad \xi_{01} \le \theta_i(\phi) \le \xi_{11} \quad or \\ & \quad \dots \quad or \\ & \xi_{0n} \le \theta_i(\phi) \le \xi_{1n} \quad or \\ 0 & otherwise \end{cases} \quad (6)$$

where $\xi_{11, \dots,} \xi_{0n}$ are the angles that specify the boundaries as well as slots on the workpiece as shown in (Fig. 15). The first subscript in ξ_{ij} represents whether the insert is entering or exiting a part, i.e., i=1 for the entry and i=0 for the exit. The second subscript j stands for the jth material region in the circumferential direction.

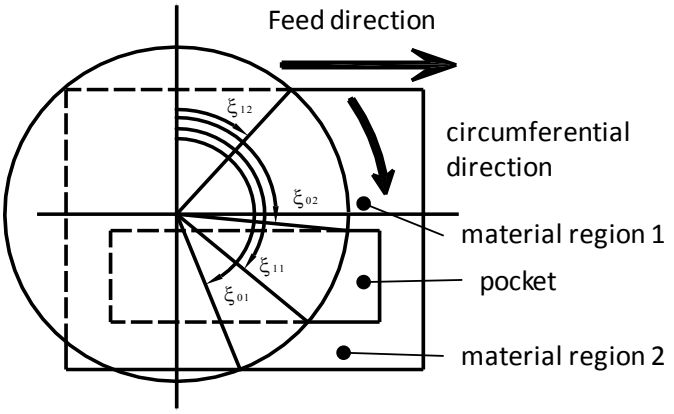

FIG. 15 CUTTER ROTATIONAL ANGLES

To focus on the variation of surface height along the cutting path, the cutter-workpiece displacement should be averaged over each cutting revolution. The cutter-workpiece displacement at a given rotational angle of cutter ϕ can first be represented by

$$\Delta h = K_d F_a = K_d \sum_{i=1}^{N} \delta(\theta_i(\phi)) F_a(i,\phi) = K_d K_a d \sum_{i=1}^{N} \delta(\theta_i(\phi)) C_i(\theta_i(\phi)) = K_d K_a d f_t \sum_{i=1}^{N} \delta(\theta_i(\phi)) \sin\theta_i(\phi) = K_1 \sum_{i=1}^{N} \delta(\theta_i(\phi)) \sin\theta_i(\phi) \quad (7)$$

where K_d is the stiffness of cutter-workpiece. All the inserts that are engaged in cutting are assumed to create the same displacement Δh. Then the average cutter-workpiece displacement of a single insert over one revolution will be the integration of Δh over the effective cutting length per revolution, i.e.,

$$\overline{\Delta h} = \frac{1}{2\pi R} K_1 \int_0^{\pi} ds = \frac{1}{2\pi} K_1 \int_0^{\pi} \sum_{i=1}^{N} \delta(\theta_i(\phi)) \sin\theta_i(\phi) d\phi \quad (8)$$

Denote $K_2 = K_1/(2\pi R) = K_d K_a d f_t/(2\pi R)$ and let

$$L = \int_0^{\pi} \sum_{i=1}^{N} \delta(\theta_i(\phi)) \sin\theta_i(\phi) d\phi$$

which can be estimated by

$$L = \sum_{i=0}^{N-1} \sum_{j=1}^{n} \int_{\xi_{1j}}^{\xi_{0j}} \delta(\theta(\phi) - \frac{2\pi}{N} i) \sin(\theta(\phi) - \frac{2\pi}{N} i) d\phi \quad (9)$$

Thus, $\overline{\Delta h} = K_2 L$. Equation (8) implies that the average cutter-workpiece displacement over one revolution is proportional to the sum of lengths of insert trajectory projected onto the direction perpendicular to the feed direction. For example, the average insert-workpiece displacement for a part as shown in Fig. 16 is

$$\overline{\Delta h} = K_2 (l_{11} + l_{21} + l_{22} + l_{15}) \quad (10)$$

where l_{ij} is the projection of the trajectory of insert i on material regions j in the circumferential direction.

In addition, the parameter K_2 derived from Eq. (8) is directly related to the depth of cut (d), feed rate (f_t), radius of cutter (R), stiffness of cutter-spindle (K_d) and cutting pressure (K_a). Therefore, K_2 has the potential as a parameter for process monitoring and will be discussed in the next section.

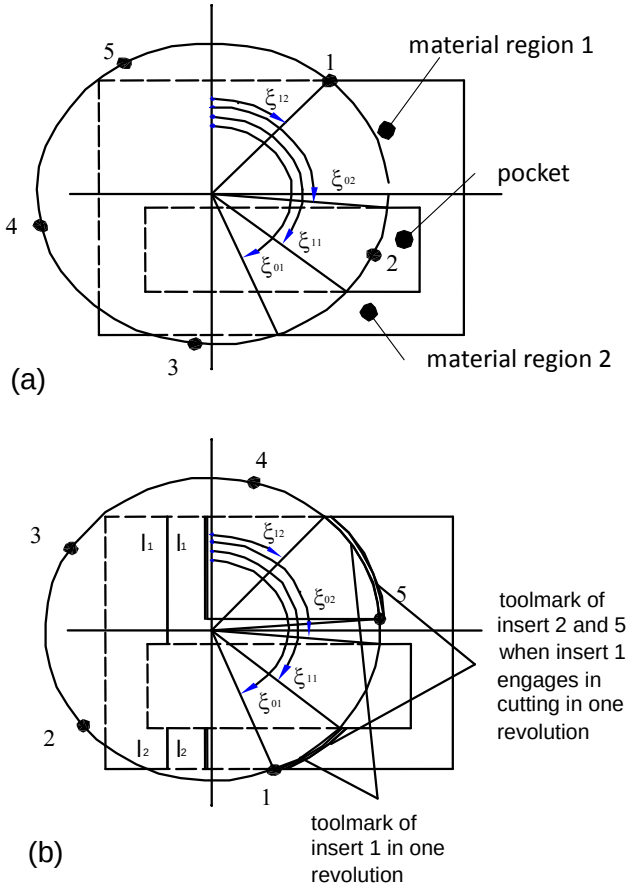

FIG. 16 AN EXAMPLE OF THE INSERT PATH (a – INSERT 1 ENTERS CUTTING, b – INSERT 1 EXISTS CUTTING)

The total length of the insert projection L can be simply approximated by the arc length of the toomark. When the number of insert is more than ten, the projection length L is proportional to the

arc length of the toolmark, as shown in Fig. 17, i.e., $L=K_3L_{arc}$, where L_{arc} is the length of toolmark and K_3 can be estimated by linear regression based on the data in Fig. 17. Table I shows a number of simulated values of K_3 given different insert numbers for Block 3. In practice, a face mill cutter may have more than 20 inserts installed and therefore this approximation is mostly applicable.

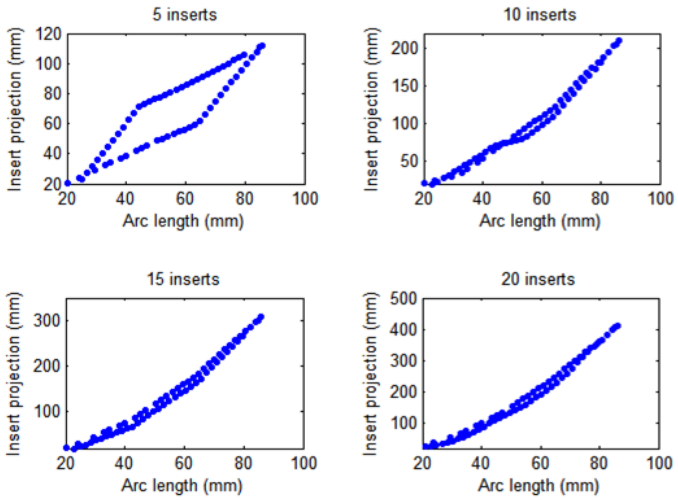

FIG. 17 THE RELATIONSHIP BETWEEN THE INSERT PROJECTION LENGTH (L) AND TOOLMARK LENGTH FOR DIFFERENT NUMBER OF INSERT (BLOCK 3)

TABLE 1. K_3 FOR DIFFERENT NUMBER OF INSERTS N (BLOCK 3)

N	10	11	12	13	14	15	16	17
K_3	3.051	3.472	3.821	4.106	4.431	4.784	5.139	5.439
N	18	19	20	21	22	23	24	25
K_3	5.745	6.069	6.410	6.745	7.040	7.360	7.700	8.016

Using the length of toolmark L_{arc}, the correlation between the MRR and surface profile can be represented in a linear form. In fact, by the definition of MRR, we have

$$MRR = L_{arc} df \tag{11}$$

So,

$$\overline{\Delta h} = K_2 L = K_2 K_3 L_{arc} = K_d K_a K_3 MRR / 2\pi RN = K_4 MRR \tag{12}$$

where $K_4 = K_d K_a K_3 / 2\pi RN$.

Model Validation

Figure 18 compares the predicted average cutter-workpiece displacement with the measured average surface profile of Block 2 and Block 3, respectively. It can be concluded that the prediction captures the jump due to the MRR variation.

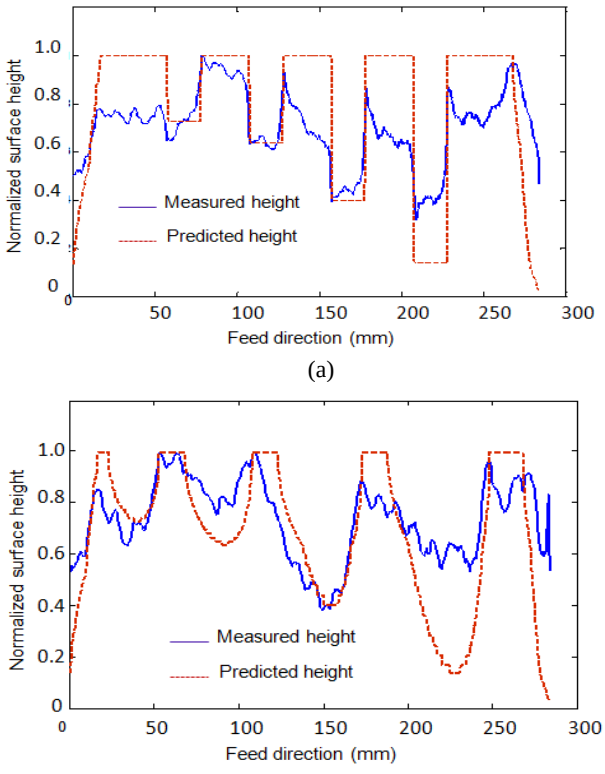

FIG. 18 COMPARISONS OF THE PREDICTED AND MEASURED AVERAGE SURFACE HEIGHT ALONG THE FEED DIRECTION ON BLOCKS 2 AND 3

Figure 19 shows the predicted axial force based on Eq. (5) on Block 1. It shows an agreement between the predicted force and extracted surface patterns in the circumferential direction (Fig. 8). The comparison of predicted force and extracted surface profile along the circumferential direction is given in Fig. 20. The abrupt changes in cutting force also match the jump locations of surface profile.

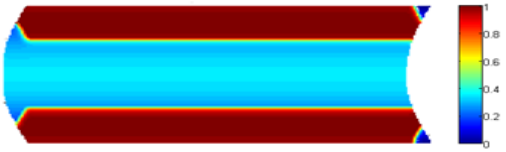

FIG. 19 THE NORMALIZED PREDICTED AXIAL CUTTING FORCE DISTRIBUTION ON BLOCK 3

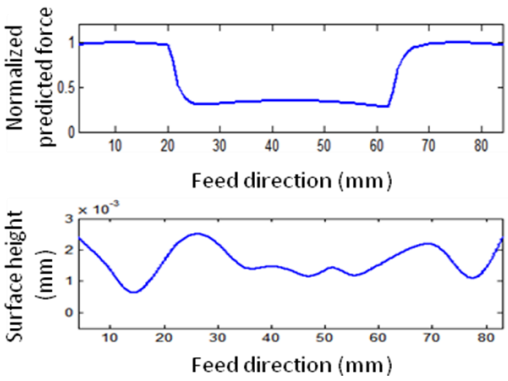

FIG. 20 A COMPARISON BETWEEN THE CUTTING FORCE AND SURFACE PROFILE ALONG THE CIRCUMFERENTIAL DIRECTION

Discussions

Figure 21 shows the relationship between the MRR and surface height for a deck face of an engine head. The cutter has 24 inserts with an effective radius of 117.7 mm. The engine head is mounted on a cast iron adapter plate during milling. The cutting process is more robust to variation sources such as vibration or fixture-induced part deformation. So, the MRR and surface height has a stronger linear correlation.

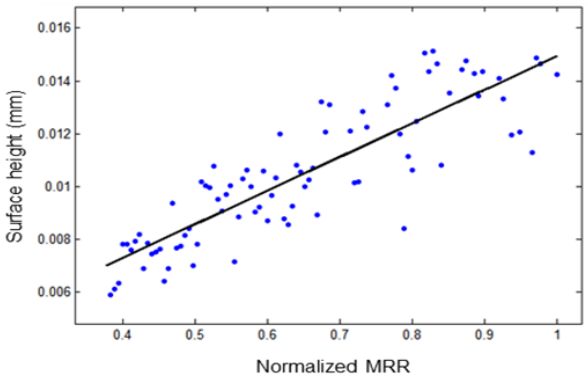

FIG. 21 A SCATTER PLOT OF THE SURFACE HEIGHT VS. MRR ON FOR AN ENGINE HEAD DECK FACE

Along the circumferential direction, the agreement between the extracted surface pattern along the circumferential direction (Fig. 8) and the cutting force distribution diagram (Fig. 19) implies that the pattern can be partially explained by the effect of cutting force changes due to the insert engagement. The discrepancy could be explained by higher order effect of dynamic cutter-workpiece system in the future study, such as using a damping and spring model.

POTENTIAL APPLICATIONS

This section discussed the potential applications of the extracted surface patterns due to cutting force dynamics in product design, machining process monitoring, and improvement.

Part design for machining. The relationship between the MRR and surface height variation can be utilized in part design. The workpiece should be designed in a way to avoid high MRR variation along the feed direction. Holes, slots, or pockets should be distributed equally over the surface, as shown in Fig. 22. Design 1 has two zones with high MRR, generating two jumps in these areas. If functional performances are not affected, the design can be improved by moving two small holes to the high-MRR area (Design 2). But the jump on the right end still exists. Design 3 has the smallest MRR variation among the three designs.

Machining improvement. Based on the linear correlation between the MRR and surface height, one can increase and reduce the feed rate to compensate for the MRR variation along the feed direction induced by surface geometry. The resultant surface profile generated by the varying-feed method as outlined in Fig. 23 is expected to exhibit less variation.

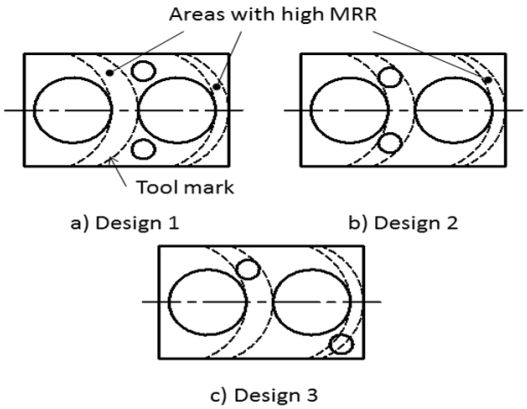

FIG. 22 PART DESIGN IMPROVEMENT FOR REDUCING THE MRR VARIATION

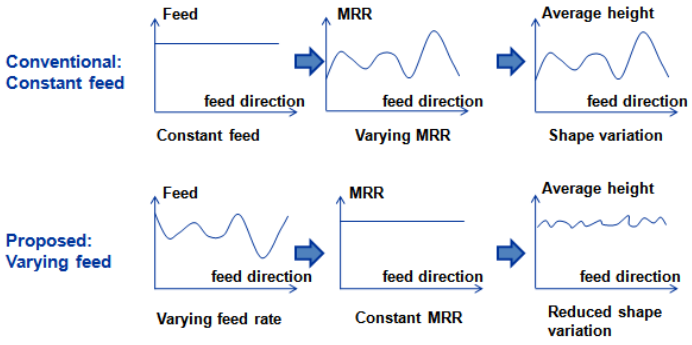

FIG. 23 SURFACE VARIATION REDUCTION USING A VARYING FEED METHOD

Another application of the MRR vs. height relationship can be in understanding and reducing the singularities on machined surfaces. Fig. 24.a shows a jump on the wing section of an engine head. Such a surface singularity is critical for the assembly between the engine head, gasket, and engine block. It is generated when the middle section of the cutter begins to hit the firing deck, thus resulting in a high MRR change along the feed direction (Fig. 24b). The MRR variation in this case could increase the flatness up to 40 microns. Using the varying-feed rate method could be effective; however, it may potentially lead to an extremely high feed rate that is able to compensate for the loss of MRR on the wing section. An alternative method can be to use a non-straight entry cutter path that mitigates the MRR variation on the wing section to reduce the jump. The detailed algorithm is being developed in another work of our related research.

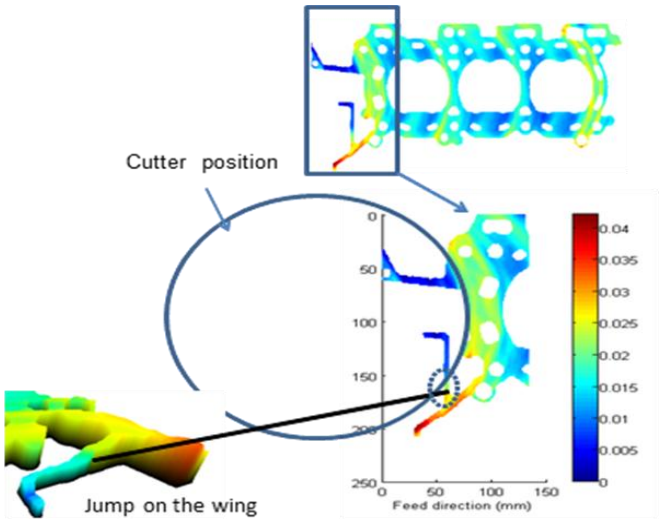

(a)

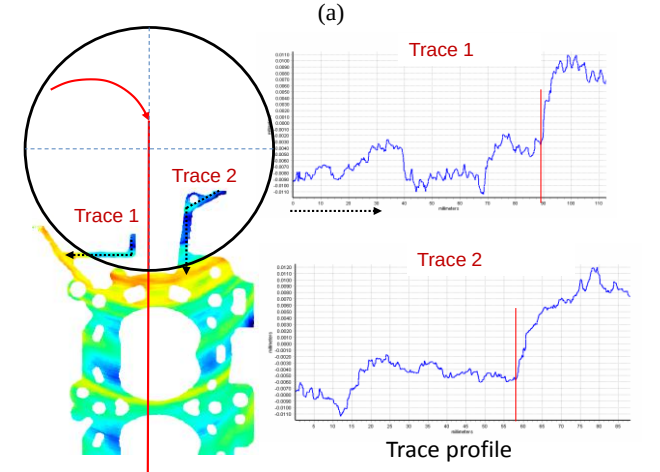

(b)

FIG. 24 AN ENGINE HEAD AND SURFACE ERROR CAUSED BY THE MRR VARIATION

Tool life monitoring. The relationship between the MRR and surface height is also influenced by the remaining tool life. Figure 25 shows that the coefficient K_4 in Eq. (12) is negatively related to the remaining tool life. Therefore, the average value of K_4 (K_2 for cutter with few inserts) contains tooling information and could be used as a parameter for monitoring tooling conditions. Another application of such a relation can be in tool replacement planning. In a CNC face milling process of automotive engine heads, engineers usually replace the face mill cutter when the jump as shown in Fig. 24 exceeds certain value of the surface span flatness specification. The new cutter is effective in bringing the jump down below the specification limit. The rationale behind this practice is that the jump on the wing section will be more significant for a worn tool since the impact (K_4) of the surface geometry (or MRR) on the surface flatness increases as the tool wears. As the tool is replaced, though the jump still exists, it is suppressed (below the specification limit) due to a reduced K_4. It can be expected that the tool life change interval could be potentially increased by appropriately selecting cutter path or feed rate.

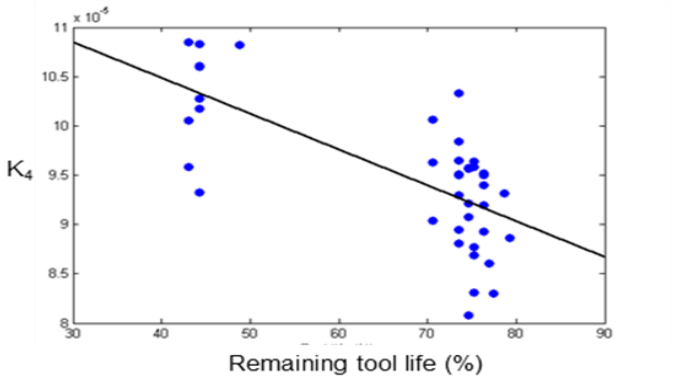

FIG. 25 K_4 VS. REMAINING TOOL LIFE

Clamping condition monitoring. The surface pattern along the circumferential direction could be useful for detecting faulty process conditions such as a clamping error. Block 1 was milled under the faulty clamping by which the part datum surface is not fully supported by the fixture. The same procedure for Fig. 8 was applied to extract the surface patterns along the circumferential direction and the result is shown in Fig. 26. It can be seen that the pattern is very different and the distance between peaks (≅42 mm) is not relatively a constant. The irregularity of the extracted patterns is related to the sensitivity of the dynamic response of cutter-workpiece system.

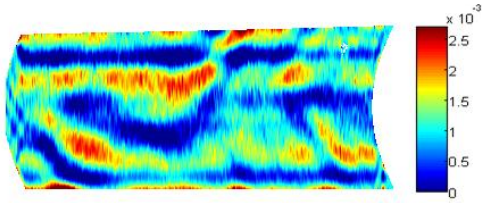

FIG. 26 THE SURFACE PATTERN INDUCED BY INSERT ENGAGEMENT VARITION UNDER A FAULTY CLAMPING CONDITION (BLOCK 1)

CONCLUSIONS

This study identified new surface variation patterns measured by the HDM along the circumferential and feed directions on a face milled surface. Cutting force modeling is conducted to interpret these surface patterns. Given the cutting conditions and surface geometry, a cutting force model is established to estimate the relative displacement of cutter-workpiece. The following conclusions are drawn from this study:

- In the circumferential direction, it is found that surface profiles are correlated to the axial cutting force. At the boundary where the number of inserts engaged in cutting changes, cutting force changes abruptly and results in jumps in the profile. This pattern is found to be sensitive to detect dynamics change of cutter-workpiece such as clamping errors.

- In the feed direction, it is found that surface variations are attributed to cutting force changes caused by the surface geometry induced MRR variations.

These findings will lead to important insights on surface design, process monitoring and improvement by maintaining a constant rate of material removal

ACKNOWLEDGMENTS

This research was supported by a NIST-Advanced Technology Program grant with the Powertrain Engineering and Manufacturing Alliance (PEMA). Mr. Tom Rothermel from Ford Motor Company and Richard Wineland from PEMA made indispensable contributions to this research.

REFERENCES

[1] Huynh, V. M., and Fan, Y., 1992, "Surface-Texture Measurement and Characterisation with Applications to Machine-Tool Monitoring," The International Journal of Advanced Manufacturing Technology, 7(1), pp. 2-10.

[2] Whitehouse, D. J., 1997, "Surface Metrology," Measurement Science and Technology, 8(9).

[3] Leith, E. N., 1997, "Overview of the Development of Holography," J. Image Sci. Technology, 41, pp. 201-204.

[4] Huang, Z., Shih, A. J., and Ni, J., 2006, "Laser Interferometry Hologram Registration for Three-Dimensional Precision Measurements," Transactions of the ASME, 128(4), pp. 887-896.

[5] Colosimo, B. M., and Senin, N., 2010, Geometric Tolerances: Impact on Product Design, Quality Inspection and Statistical Process Monitoring, Springer.

[6] Wilkinson, P., Reuben, R. L., Jones, J. D. C., Barton, J. S., Hand, D. P., Carolan, T. A., and Kidd, S. R., 1997, "Surface Finish Parameters as Diagnostics of Tool Wear in Face Milling " Wear, 205(1-2), pp. 47-54.

[7] Liao, Y., Stephenson, D. A., and Ni, J., 2009, "Assessment of Tool Wear Based on Surface Texture Parameters," ASME 2009 International Manufacturing Science and Engineering Conference, 2, pp. 463-470.

[8] Schmitz, T. L., Couey, J., Marshb, E., Mauntler, N., and Hughes, D., 2006, "Runout Effects in Milling: Surface Finish, Surface Location Error, and Stability " International Journal of Machine Tools & Manufacture, 47(5), pp. 841-851.

[9] Baek, D. K., Ko, T. J., and Kim, H. S., 1997, "A Dynamic Surface Roughness Model for Face Milling," Precision Engineering, 20(3), pp. 171-178.

[10] Kline, W. A., and DeVor, R. E., 1983, "The Effect of Runout on Cutting Geometry and Forces in End Milling," International Journal of Machine Tool Design and Research, 23(1-2), pp. 123-140

[11] Sutherland, J. W., and DeVor, R. E., 1986, "Improved Method for Cutting Force and Surface Error Prediction in Flexible End Milling Systems," ASME Journal of Engineering for Industry, 108(4), pp. 269-279.

[12] Takeuchi, Y., and Sakamoto, M., 1964, "Analysis of Machining Error in Face Milling," Proceedings of the International Machine Tool Design and Research Conference.

[13] Camelio, J., Hu, S. J., and Zhong, W., 2004, "Diagnosis of Multiple Fixture Faults in Machining Processes Using Designated Component Analysis," Journal of Manufacturing Systems, 23(4), pp. 309-315.

[14] Liao, Y. G., and Hu, S. J., 2001, "An Integrated Model of a Fixture-Workpiece System for Surface Quality Prediction," International Journal of Advanced Manufacturing Technology, 17(11), pp. 810-818.

[15] Gu, F., Melkote, S. N., Kapoor, S. G., and DeVor, R. E., 1997, "A Model for the Prediction of Surface Flatness in Face Milling," Journal of Manufacturing Science and Engineering 119(4A), p. 9.

[16] Ruzhong, Z., Wang, K. K., and Merchant, E., 1983, "Modelling of Cutting Force Pulsation in Face-Milling " CIRP Annals - Manufacturing Technology, 32(1), pp. 21-26.

[17] Wang, J.-J. J., Liang, S. Y., and Book, W. J., 1995, "Convolution Analysis of Milling Force Pulsation," ASME Journal of Engineering for Industry, 116(1), pp. 17-25.

[18] Andersson, C., Andersson, M., and Ståhl, J.-E., 2010, "Experimental Studies of Cutting Force Variation in Face Milling," International Journal of Machine Tools & Manufacture, 51(1), pp. 67-76.

[19] Li, X. P., Zheng, H. Q., Wong, Y. S., and Nee, A. Y. C., 2000, "An Approach to Theoretical Modeling and Simulation of Face Milling Forces " Journal of Manufacturing Processes, 2(4), pp. 225-240.

[20] Wu, D. W., 1989, "A New Approach of Formulating the Transfer Function for Dynamic Cutting Processes," ASME Journal of Engineering for Industry, 111, pp. 37-47.

[21] Montgomery, D., and Altintas, Y., 1991, "Mechanism of Cutting Force and Surface Generation in Dynamic Milling," Transactions of the ASME, 113(5), p. 160.

[22] 2003 Surface Texture, Surface Roughness, Waviness and Lay: ASME B46.1-2002 American Society of Mechanical Engineers

[23] Raja, J., Muralikrishnan, B., and Fu, S., 2002, "Recent Advances in Separation of Roughness, Waviness and Form," Precision Engineering, 26(2), pp. 222-235.

[24] Fu, H. J., Devor, R. E., and Kapoor, S. G., 1984, "A Mechanistic Model for the Prediction of the Force System in Face Milling Operations," Transactions, ASME J. Eng. for Industry 106, pp. 81-88.